atmosphere

MDPI

Article

Analysis of the Meteorological Conditions and Atmospheric Numerical Simulation of an Aircraft Icing Accident

Haoya Liu [1,2], Shurui Peng [3], Rong Fang [4], Yaohui Li [1,2], Lian Duan [1,2], Ten Wang [1], Chengyan Mao [5,*] and Zisheng Lin [6,*]

[1] College of Aviation Meteorology, Civil Aviation Flight University of China, Guanghan 618307, China; liuhy@cafuc.edu.cn (H.L.); li-yaohui@163.com (Y.L.); cafcdl@sina.com (L.D.); wangt75@mail2.sysu.edu.cn (T.W.)
[2] China Meteorological Administration Key Laboratory for Aviation Meteorology, Guanghan 618307, China
[3] China Civil Aviation East China Air Traffic Administration Jiangxi Branch, Nanchang 330117, China; pengshurui@163.com
[4] Discipline Construction Office, Civil Aviation Flight University of China, Guanghan 618307, China; fangr5@cafuc.edu.cn
[5] Quzhou Meteorological Bureau, Quzhou 324000, China
[6] Planetary Environmental and Astrobiological Research Laboratory (PEARL), School of Atmospheric Sciences, Sun Yat-sen University, Zhuhai 519082, China
* Correspondence: maochy@mail3.sysu.edu.cn (C.M.); linzsh5@mail2.sysu.edu.cn (Z.L.)

Abstract: With the rapid development of the general aviation industry in China, the influence of high-impact aeronautical weather events, such as aircraft icing, on flight safety has become more and more prominent. On 1 March 2021, an aircraft conducting weather modification operations crashed over Ji'an City, due to severe icing. Using multi-source meteorological observations and atmospheric numerical simulations, we analyzed the meteorological causes of this icing accident. The results indicate that a cold front formed in northwestern China and then moved southward, which is the main weather system in the icing area. Based on the icing index, we conducted an analysis of the temperature, relative humidity, cloud liquid water path, effective particle radius, and vertical flow field, it was found that aircraft icing occurred behind the ground front, where warm-moist airflows rose along the front to result in a rapid increase of water vapor in 600–500 hPa. The increase of water vapor, in conjunction with low temperature, led to the formation of a cold stratiform cloud system. In this cloud system, there were a large number of large cloud droplets. In addition, the frontal inversion increased the atmospheric stability, allowing cloud droplets to accumulate in the low-temperature region and forming meteorological conditions conducive to icing. The Weather Research and Forecasting model was employed to provide a detailed description of the formation process of the atmospheric conditions conducive to icing, such as the uplifting motion along the front and supercooled water. Based on a real case, we investigated the formation process of icing-inducing meteorological conditions under the influence of a front in detail in this study and verified the capability of a numerical model to simulate the meteorological environment of frontal icing, in order to provide a valuable reference for meteorological early warnings and forecasts for general aviation.

Keywords: aircraft icing; cold front; general aviation; atmospheric numerical simulation

Citation: Liu, H.; Peng, S.; Fang, R.; Li, Y.; Duan, L.; Wang, T.; Mao, C.; Lin, Z. Analysis of the Meteorological Conditions and Atmospheric Numerical Simulation of an Aircraft Icing Accident. *Atmosphere* **2024**, *15*, 1222. https://doi.org/10.3390/atmos15101222

Academic Editors: Duanyang Liu, Hongbin Wang and Shoupeng Zhu

Received: 24 August 2024
Revised: 2 October 2024
Accepted: 5 October 2024
Published: 14 October 2024

1. Introduction

Aircraft icing refers to the phenomenon where ice accumulates on the surface of an aircraft due to the freezing of supercooled water droplets and the condensation of water vapor [1,2]. When ice forms on the leading edge of the wings or tail, it can rapidly deteriorate the aerodynamic performance of the aircraft. Ice forming on the engine intake or detached ice entering the engine can lead to a rapid decrease in engine efficiency. Furthermore, protruding navigation instruments and radio communication equipment

may malfunction due to ice coverage, and severe icing can increase the local weight, thereby altering the center of gravity of the aircraft [3–6]. The above effects of icing can negatively affect the stability and maneuverability of an aircraft, posing significant threats to flight safety. In extreme cases, it can lead to catastrophic accidents, earning it the title of the "invisible killer" of flight safety [7,8].

There are many factors affecting aircraft icing, including flight speed, aircraft shape, and the shape of external equipment [9,10]. However, the most essential one is the meteorological condition in the area where the aircraft operates [1,11]. Studies have shown that meteorological elements related to icing include air temperature, humidity, vertical velocity, atmospheric stability, supercooled water content, supercooled droplet size, and atmospheric impurities [12–15]. When an aircraft enters a cold cloud system or stays in a cold and moist environment for a long time, supercooled water droplets continuously collide with the aircraft surface, leading to icing. Especially when the temperature of the aircraft surface is lower than the ambient dew point temperature, water vapor in the atmosphere can also condense into ice on the aircraft surface. Therefore, the meteorological conditions for ice formation are also diverse [1,16,17]. To objectively describe the meteorological conditions that lead to icing, a variety of icing indices have been proposed and are widely used in forecasting icing potential. The icing index recommended by the International Civil Aviation Organization is the most commonly used. This index considers the two main meteorological elements for the formation of supercooled liquid water, namely temperature and humidity [18]. Based on this, considering the different meteorological conditions for icing in different regions, some improved icing indices are used for specific regional studies, such as the Simplified Forecast Icing Potential index, Research Application Program index, National Aviation Weather Advisory Unit index, and the Air Force Global Weather Central Rawinsonde Observation index [19–21].

Most of the research on the meteorological conditions of icing is based on the icing records from pilot reports or the calculation of icing indices to determine icing areas. Then, the weather systems affecting the region are analyzed in detail. Based on an icing case and using observations and numerical simulations, Fernández-González et al. [22] verified that in atmospheric layers with weak inversion, ascending motions caused by terrain and cyclones are conducive to the formation of supercooled large droplets. Reinking et al. [23] found that the undulating updrafts generated by gravity waves on the leeward side of mountains favor water vapor condensation, which increases and maintains the content of liquid water in clouds and also makes the formation of supercooled droplets possible in a relatively low-temperature environment. Compared with troughs, surface low pressure and atmospheric fluctuations, frontal weather systems are the most common cause of aircraft icing [24]. Politovich and Bernstein [25] carried out a synoptic analysis of icing events in Colorado over five years and found that about 25% of icing events were associated with fronts. Previous studies have indicated that temperature decrease caused by cold fronts and the climbing of warm-moist airflow caused by cold and warm fronts can carry high-humid airflow to the upper part of cold air on the surface, forming a lot of supercooled droplets and the icing atmospheric environment [24–29]. However, it is obvious that not all frontal processes are accompanied by the formation of icing conditions. Therefore, at different locations and under different atmospheric backgrounds, different frontal characteristics determine whether icing conditions can form. The weather and climate characteristics are complex and diverse in China. Aircraft icing events occur frequently and show remarkable seasonal and regional characteristics [30,31]. Previous studies have indicated that icing events in China are associated with various weather systems, such as cold fronts, upper-level troughs, shear lines, surface high pressure, inverted troughs, extratropical cyclones, and low-level jets. Among all, frontal systems are still the major weather system for icing formation [32–36]. Based on airborne cloud physical detection data, satellite remote sensing data, and reanalysis data, the icing events associated with frontal weather systems in Gansu Province [33], Anhui Province [34], Shaanxi Province [36], and Xinjiang Uygur Autonomous Region [37] were analyzed, and the results indicated that the stratocumulus

clouds near fronts usually have high content of supercooled water, which facilitates the formation of icing.

Regarding aircraft icing forecasts, icing potential forecasts based on mesoscale numerical models are one of the main methods [13,38,39]. Davis et al. [40], Merino et al. [13], and Guo et al. [41] used the Weather Research and Forecasting (WRF) model to simulate the atmospheric environment of aircraft icing events in Sweden, the Iberian Peninsula, and the United States, respectively. Their results showed that the WRF model can better describe the atmospheric environment where icing occurs, with appropriate parameter settings. However, in different regions and under the influence of different weather systems, the model parameters are not exactly the same. Especially, there are relatively few numerical simulations of icing events in China [42]. Besides, with the rapid development of the general aviation industry in China, the volume of general aviation operations has increased dramatically, but there are relatively few aircraft anti-icing and deicing methods in general aviation. Moreover, these aircraft often operate in altitudes between 2000 m and 6000 m, where icing forms extremely easily. Addressing the significant threat icing poses to general aviation flight safety is an urgent issue [1,43]. Therefore, for general aviation, conducting synoptic analysis and numerical simulations of icing meteorological conditions under the influence of frontal weather systems has crucial practical value in enhancing meteorological support capabilities for general aviation.

The remainder of this paper is organized as follows. Section 2 introduces the data and methods used in this study. Sections 3 and 4 provide the synoptic analysis and numerical simulations of meteorological conditions for aircraft icing. The main conclusions are presented in Section 5.

2. Data and Methods

2.1. Data

The case originates from the official accident investigation report of the Aviation safety information system of the Civil Aviation Administration of China (CAAC) (https://safety.caac.gov.cn/indexnewsdetail/init.act?args=d4b0cc393015415baf2785963e251d22 (accessed on 10 May 2024)). The report provides a detailed account of an aircraft crash caused by icing, which occurred over Ji'an City, Jiangxi Province at 15:00 BJT (Beijing Standard Time) on 1 March 2021. Specifically, a BE300 propeller aircraft conducting cloud seeding operations experienced severe wing and propeller icing despite its deicing systems functioning normally. Prolonged flight in an icing environment (more than 15 min, with an airspeed of about 150 nmi/h) led to the aircraft stalling and entering a spiral dive, ultimately crashing and causing the death of all five people on board. The accident report recorded the icing time, location, and height, but did not analyze the meteorological reasons for the icing.

The atmospheric circulation and the weather system during this icing event are analyzed by using European Center for Medium-Range Weather Forecasts fifth-generation reanalysis data (ERA5, https://cds.climate.copernicus.eu/cdsapp#!/dataset/reanalysis-era5-pressure-levels?tab=overview (accessed on 10 May 2024)) [44]. During the production of this reanalysis dataset, a large amount of aircraft observations were assimilated, and it has been indicated that the dataset can accurately describe the atmospheric environment for icing formation [45,46]. In this dataset, the elements selected in this research for analysis are hourly temperature, humidity, specific humidity, vertical velocity, and geopotential height, from the surface layer to 450 hPa, with a spatial resolution of $0.125^\circ \times 0.125^\circ$. Moreover, the satellite data from the Moderate-resolution Imaging Spectroradiometer (MOD08-D3, https://atmosphere-imager.gsfc.nasa.gov/products/daily (accessed on 10 May 2024)) and the sounding data from the nearest meteorological station, i.e., Nanchang station, (about 200 km north of Ji'an City) are used in this study.

2.2. Model

In order to describe the atmospheric conditions for icing formation in more detail, the WRF model (version 4.3.3) is used to simulate this icing process [47]. Two nested grids are set in this model (Figure 1). The resolution of the inner grid is 3 km, and the vertical layers are 42, up to 50 hPa. The simulation period is from 00:00 BJT on 27 February to 18:00 BJT on 1 March 2021. Taking the model settings of Merino et al. [13], Bolgiani et al. [48], and Liu et al. [49] as references when simulating the supercooled water in clouds, the main physical parameters of the WRF model used in this research are shown in Table 1. The parameterization scheme selected in Table 1 is listed below: Morrison 2-mom microphysics scheme (Mp_Physics = 10), Kain-Fritsch cumulus parameterization scheme (Cu_Physics = 1), RRTM longwave radiation scheme (Ra_lw_Physics = 1), Dudhia shortwave radiation scheme (Ra_sw_Physics = 1), YSU planetary boundary layer schemes (Bl_pbl_Physics = 1), Eta similarity surface layer scheme (Sf_sfclay_Physics = 1), and Noah land-surface model (Sf_surface_Physics = 2). The Cudt and Radt options are used to control the time intervals of cumulus parameterization and radiation physics, respectively, and we set the Icloud option to 1 to account for the impact of the cloud on radiation physics.

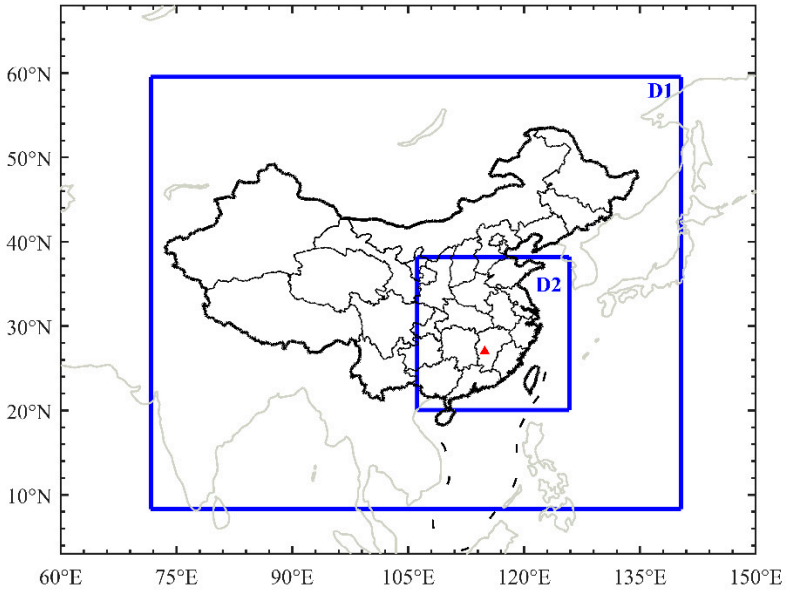

Figure 1. Simulation region by using the Weather Research and Forecasting (WRF) model. D1 and D2 denote the outer and inner nested grids, with spatial resolutions of 9 km and 3 km, respectively, and the red triangle represents the location of the aircraft icing accident.

Table 1. Parts of the physical parameters in the WRF model.

WRF Physic Options	Domain 1	Domain 2
Mp_Physics	10	10
Cu_Physics	1	1
Ra_lw_Physics	1	1
Ra_sw_Physics	1	1
Bl_pbl_Physics	1	1
Sf_sfclay_Physics	1	1
Sf_surface_Physics	2	2
Radt	15	15
Cudt	0	0
Icloud	1	

2.3. Icing Index

Previous studies have suggested that the icing index recommended by the International Civil Aviation Organization (hereafter referred to as the Ic index) can well describe the icing meteorological environment in China [50,51]. This index is also used in this research to capture the icing meteorological environment in the area of the aircraft icing accident. The algorithm is as expressed by Equation (1).

$$\mathbf{Ic} = [(\mathbf{RH} - \mathbf{50}) \times \mathbf{2}] \times [\boldsymbol{t} \times (\boldsymbol{t} + \mathbf{14})/(-\mathbf{49})] \quad (1)$$

where "Ic" indicates the icing index, RH the relative humidity, and t the temperature (°C). Therefore, by utilizing gridded relative humidity and temperature fields from the ERA5 reanalysis data, we can readily obtain the Ic index at various locations and altitudes. It can be seen that the Ic index reflects the most critical atmospheric temperature and humidity conditions for icing formation. When the relative humidity is larger than 50% and the temperature is between 0 °C and −14 °C, the Ic index is positive, which characterizes the beneficial meteorological conditions conducive to icing formation. According to practical experience, when the Ic index is equal to or greater than 50, moderate icing can form, and when the value is equal to or greater than 80, the icing that forms in this atmospheric environment can reach severe icing.

3. Synoptic Analysis of Meteorological Conditions for Aircraft Icing

3.1. Overview of the Aircraft Icing Accident

According to the accident investigation report, the aircraft encountered severe icing in altitudes of 4800–5100 m from 15:00 BJT to 15:18 BJT on 1 March 2021, ultimately entering a high-speed spiral descent and crashing in Ji'an City, Jiangxi Province (115° E, 27° N). The report mentions that during this period, there were no obvious cumulus convective activities in the accident location. It was this seemingly low-risk icing environment that ultimately led to the accident. Therefore, we conducted a detailed analysis of the specific meteorological conditions for the icing accident.

3.2. Main Weather System over the Aircraft Icing Region

Firstly, weather maps drawn with the ERA5 reanalysis dataset are used to analyze the main weather system over the icing region and its evolution process, as shown in Figure 2. The results indicate that at 20:00 BJT on 28 February, before the icing accident (Figure 2a), the circulation pattern in East Asia was characterized by a cold vortex at high latitudes to the north of Lake Baikal. The cold vortex facilitated the southward movement of cold air originating from central Siberia towards Shaanxi Province along the southeastern flank of the Tibetan Plateau. At 550 hPa (Figure 2a), in northern China, the southern branch trough east of the Qinghai-Tibet Plateau superimposed in the same phase with the northern branch trough. A strong southward cold advection formed behind the trough, providing low-temperature conditions for the icing formation in the subsequent accident location. At this moment, the temperature at 500 hPa over northern Jiangxi Province was lower than −10 °C, while the cold airflow had not arrived at Ji'an City where the air temperature was between 0 and −4 °C. Meanwhile, in the region ahead of the southern branch trough in Hunan and Jiangxi provinces, strong winds of 22 m/s occurred, forming a southwest jet at high altitudes. This jet blocked cold air moving southward, resulting in the gathering of cold air from Qinghai to Shaanxi to form a dense band of isotherms, which indicates the frontogenesis of a weak cold front. In lower layers during the same period (Figure 2d), a cold high-pressure center was located in central Xinjiang. Cold and warm air masses confronted each other near 28°N. The dense bands of isoheight contours and isotherms formed a more pronounced frontal zone. Affected by the southwest vortex, there was a low-level jet developing over the southeastern Sichuan Basin, bringing water vapor from the South China Sea to Jiangxi Province, which provided favorable moisture conditions for icing formation. On the ground (Figure 2g), the cold front represented by the 1020 hPa

isobar was located in the north of Hubei Province. The temperature difference between the front and its rear reached 6 °C. Therefore, this process is defined as a weak cold frontal process. At this time, Ji'an City was located in the warm airflow in front of the front, where the temperature dew point difference was about 3 °C, which indicates that the water vapor conditions were sufficient on the ground.

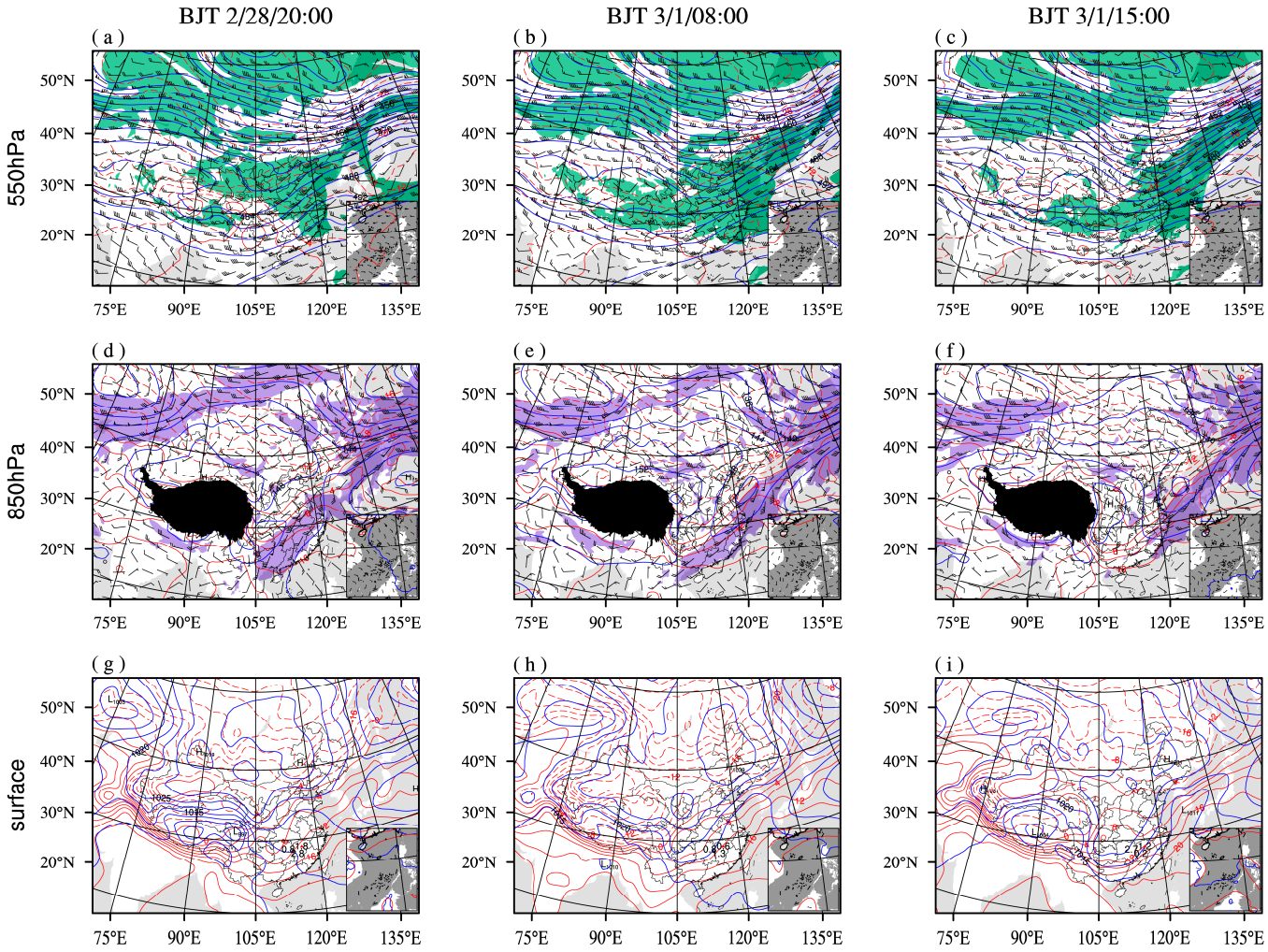

Figure 2. Atmospheric circulation situation before and at the time of the icing accident: (**a**–**c**) 550 hPa and (**d**–**f**) 850 hPa geopotential height, temperature, and wind fields, as well as (**g**–**i**) surface pressure and temperature fields at (**a**,**d**,**g**) 20:00 BJT (Beijing Standard Time) on 28 February, (**b**,**e**,**h**) 08:00 BJT on 1 March and (**c**,**f**,**i**) 15:00 BJT on 1 March. The blue lines in (**a**–**f**) represent the isoheight contours (interval of 4, unit: 10 gpm). The green shaded areas in (**a**–**c**) indicate the relative humidity larger than 60%, the purple shaded areas in (**d**–**f**) denote the wind speed larger than 12 m/s, and the blue lines in (**g**–**i**) represent the isobars (interval of 5, unit: hPa). "H" and "L" represent the high- and low-pressure centers, respectively. The red contours indicate the isotherms (interval of 4, unit: °C), where solid and dotted lines denote the positive and negative values. The red triangles in (**g**–**i**) show the location of the aircraft icing accident.

At 08:00 BJT on 1 March, in the middle and upper troposphere (Figure 2b), the Southern Branch Trough and Northern Branch Trough in the mid-latitude region strengthened. The cold air guided by the Northern Branch Trough became stronger, and the 0 °C isotherm moved southward, resulting in the temperature over Ji'an City decreasing to between −4 °C and −8 °C. Meanwhile, the cold high pressure at low levels strengthened and moved southward (Figure 2e). The cold front had arrived in the north of Jiangxi. As the

southwest vortex weakened and dissipated, the southwesterly jet over southern Jiangxi was weakened and tended to disappear, and only part of it remained in central Jiangxi and continued to supply water vapor. However, the weakening of the southwest vortex was beneficial to the continuous southward movement of cold air. As shown in the surface synoptic chart (Figure 2h), the surface cold air (1020 hPa isobar) had arrived in the north of Jiangxi. Compared with the temperature on the previous day, the air temperature at Nanchang station in Jiangxi dropped by about 1 °C, and the dew point temperature difference dropped to 1 °C. This situation indicates that the air temperature continued to decrease, and the atmosphere became more saturated.

At 15:00 BJT on 1 March, when the incident happened, the mid-latitude trough and ridge strengthened (Figure 2c), further driving the southward movement of cold air behind the trough. The upper-level wind diverged, leading to the upward transport of water vapor at lower levels. The cold high moved eastward to the Hetao area (Figure 2f), and Jiangxi was located in the northerly airflow in front of the high-pressure system, where the cold advection was quite strong. Cold air had entered northern Jiangxi, and there was still southwesterly airflow supplying water vapor continuously to southern Jiangxi. Ji'an was located on the cold shear line of northwesterly and southwesterly wind. This situation favored the vertical upward transport of water vapor at lower levels. Moreover, the temperature decrease contributed to the relative humidity increase, facilitating icing formation. The surface weather chart (Figure 2i) suggests that by the time of the incident, the main section of cold air had advanced southward to the north of the Nanling Mountains. At this time, cold air had already started to influence northwestern Jiangxi, resulting in 1 °C temperature decrease and precipitation at Nanchang station. The cold front influenced Ji'an City.

In conjunction with the weak cold front moving from the northwest to the southeast of China, the corresponding variations in the high-value area of the Ic index are analyzed to reflect the relationship between the front and the meteorological environment of icing formation. From the spatial distribution of the Ic index at 550 hPa from 23:00 BJT on 28 February to 15:00 BJT on 1 March (Figure 3a–c), it can be found that with the eastward and southward movement of cold air (as shown in Figure 2), the severe icing potential area (Ic index > 80) gradually moved from Hubei and Hunan to Jiangxi Province, and thus a high-value center appeared at the time and location corresponding to the icing accident. The time-longitude profile of the Ic index (Figure 3d) suggests that the icing area moved from west to east in synchronization with cold air. The above correspondence not only reflects the accuracy of the Ic index in indicating the icing areas, but also, more importantly, reflects the relationship between the cold frontal process and the icing formation. Furthermore, the 550 hPa temperature over the incident location gradually increased with time (solid green line in Figure 3e), which is related to the arrival of warm air before the cold front. However, in terms of the temperature value, the upper-level temperature was below 0 °C on the day of the incident, and at 15:00 BJT of that day, the upper-level temperature was −7 °C. Therefore, although the warm air ahead of the cold front did contribute to a temperature increase, the magnitude of this increase was not substantial, and the 550 hPa temperature remained within a range conducive to icing. This is a key factor in satisfying the temperature conditions necessary for icing in the atmosphere. For humidity conditions (Figure 3f), the relative humidity variation closely resembled the pattern of the Ic index (Figure 3d) in the incident location. The saturation degree of the atmosphere increased continuously over the incident location, from 60% to about 100%, providing sufficient water vapor for atmospheric icing conditions. Therefore, the low-temperature and high-humidity conditions suitable for icing near the altitude of 5000 m recorded in the investigation report of this icing accident are closely related to the cold frontal process.

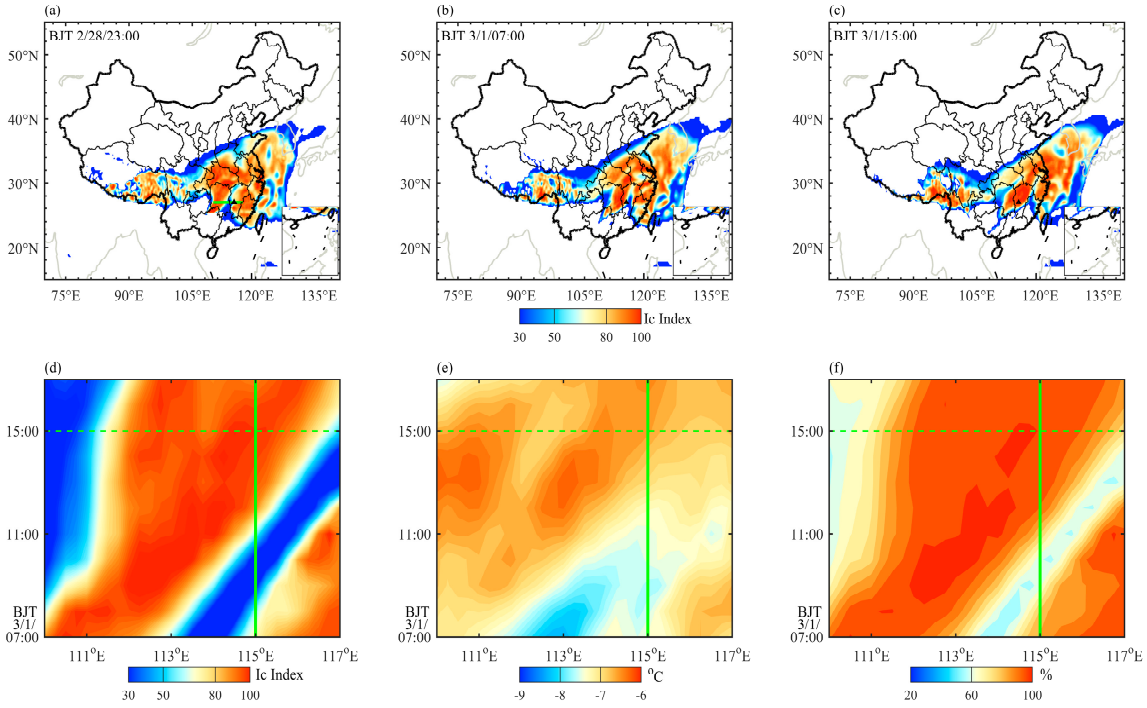

Figure 3. Spatial distribution of the 550 hPa Ic index at (**a**) 23:00 BJT on 28 February, (**b**) 07:00 BJT on 1 March, and (**c**) 15:00 BJT on 1 March, and time-longitude profiles of the (**d**) Ic index, (**e**) temperature and (**f**) relative humidity at 550 hPa. The green short line in (**a**) shows the latitudinal position of the time-longitude profiles in (**d**–**f**), the black triangles represent the accident location, and the green solids and dotted lines in (**d**–**f**) show the longitude of the accident location and the time of the accident, respectively.

The accident investigation report indicates that when the pilot first activated the deicing equipment, the aircraft remained at an altitude of 4800 m. After performing eight deicing operations, the aircraft climbed to 5100 m, but severe icing persisted, eventually leading to the aircraft disengaging from autopilot, starting to roll, and diving at this altitude. Therefore, it is greatly significant to acquire knowledge of the height and thickness of the icing layer to timely escape the danger zone after icing occurs. Figure 4 presents the altitude-time profiles of the Ic index, temperature, and relative humidity. As shown in Figure 4a, the Ic index over Ji'an City gradually increased with the approach of the cold front from 11:00 BJT on 1 March and reached the maximum at 15:00 BJT. Note that the large-value areas of the Ic index appeared in the altitudes of 600–550 hPa, indicating a moderate to severe icing risk for flights within this region, which aligns well with the actual icing altitude in the incident report. Further analysis of air temperature and humidity is conducted to explore the reasons for the high-value areas of the Ic index. As shown in Figure 4b, it can be found that in the altitude range of 600–550 hPa over the incident location, during 11:00–15:00 BJT on 1 March, the temperature increased from −10 °C to −8 °C, which is consistent with the result in Figure 3e. It is evident that the increase in Ic index in 600–550 hPa at 15:00 BJT was not primarily attributed to temperature decrease. However, it is important to note that, when compared with the limiting icing envelope delineated in 14 CFR Part 25 Appendix C (FAA requirements for aircraft icing certification), the actual ambient temperature at the incident altitude (about 18,000 ft) is around −9 °C, which is well within the defined icing envelope (specifically Figure 2: Continuous maximum (stratiform clouds) atmospheric icing conditions ambient temperature vs. pressure altitude in 14 CFR Part 25 Appendix C). This signifies that, possibly the icing conditions during the accident were challenging for the aircraft's anti-icing and de-icing system. Moreover, the temperature variance beneath 700 hPa suggests that the air temperature decreased remarkably from 11:00 BJT to 15:00 BJT. From 13:00 BJT, a prominent frontal inversion layer appeared at around 850 hPa, showing

distinct cold front characteristics. The altitude–time profile of the relative humidity over the incident location (Figure 4c) shows that as the cold front advanced, the high-value region of the relative humidity rapidly rose from below 700 hPa at 11:00 BJT to 550 hPa at 15:00 BJT. The warm-moist airflow ahead of the front provided abundant water vapor to the low-temperature zone from lower to upper levels, creating icing meteorological conditions at the altitude of the accident.

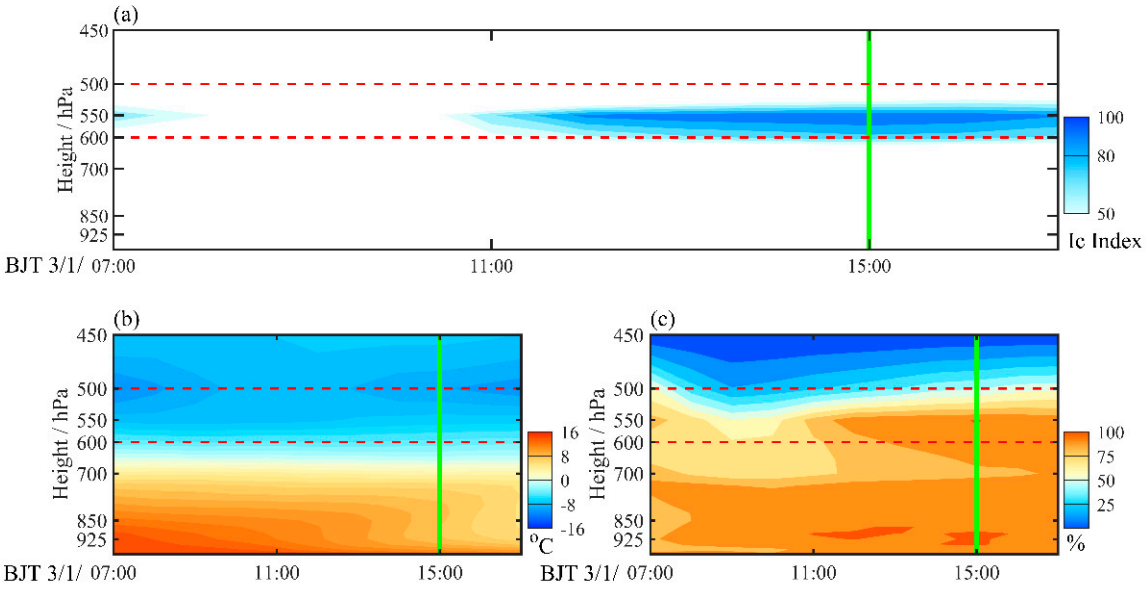

Figure 4. Altitude-time profiles of the (**a**) Ic index, (**b**) temperature, and (**c**) relative humidity. The green solid lines indicate the time of the icing accident, and the red dotted lines represent the heights of 600 hPa and 500 hPa.

The 24 h temperature variation (Figure 5a) and 3 h temperature variation (Figure 5b) demonstrate that the icing at 15:00 BJT on 1 March happened in the negative temperature variation area behind the cold front. Compared with the noticeable temperature decrease on the ground frontal line, the area behind the front was more characterized by the lifting of warm airflow along the front. The above analyses clearly reveal that the cold front is the main weather system causing the icing accident. Moreover, the rise of warm air caused by the front leads to water vapor increase at upper levels, which is more critical than the temperature decrease caused by the cold front. This conclusion well explains why not all cold front weather processes can give rise to an atmospheric icing environment. The reason lies in that the temperature drop in the rear of the cold front is mainly manifested in the lower atmosphere, while it has less influence on the temperature of the middle and upper atmosphere, and there is even a slight temperature rise. The formation of the atmospheric icing environment is mainly attributed to the increase in water vapor in the original high-altitude cold environment. Therefore, it can be postulated that when the low-level water vapor is abundant enough and the upward transportation of water vapor is strong enough, even weak cold front processes or warm front processes can give rise to an atmospheric icing environment.

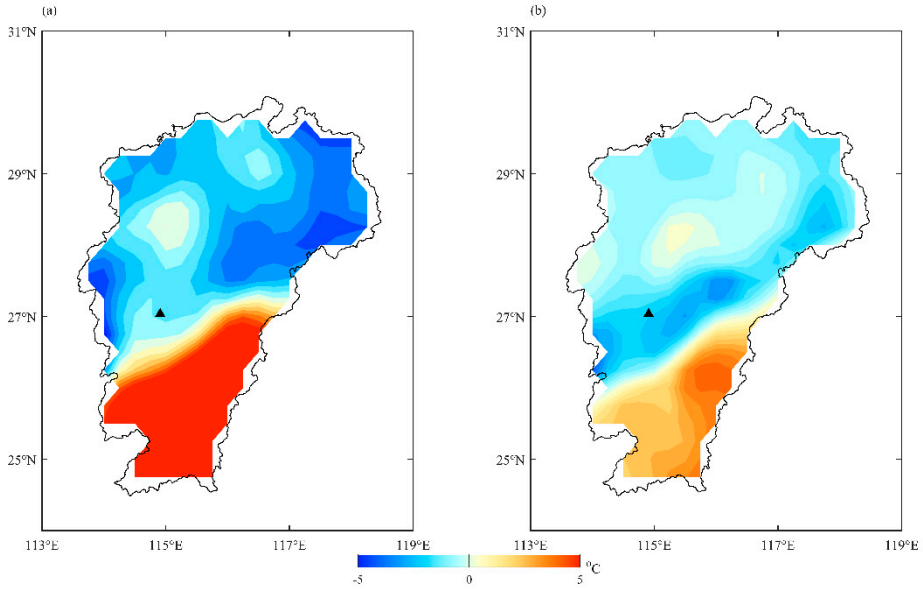

Figure 5. (**a**) Past 24 h and (**b**) 3 h temperature difference at 15:00 BJT on 1 March. The black triangles represent the location of the icing accident.

Based on satellite remote sensing data, the characteristics of hydrometeors in the cold front cloud system, which is caused by the uplift of warm-moist airflow, can be identified. The cloud liquid water path can represent the total liquid water content in the vertical atmospheric column, which is often used to reflect the supercooled water content in clouds. Figure 6 presents the spatial distributions of the cloud liquid water path, effective particle radius, cloud top temperature, and optical thickness. As presented in Figure 6a, the cloud liquid water path at the location of the incident exceeds 700 g/cm^2, indicating a high-humidity environment. The accumulation of a large amount of liquid water vapor in cold clouds can produce sufficient supercooled water. Once this liquid water vapor touches the surface of the aircraft, serious icing can occur. In terms of the liquid water content (Figure 4c), the formation of its high-value areas in clouds is related to the rapid increase of relative humidity at the icing altitude, which is the result of water vapor lifting along the front to condense liquid water. Effective particle radius can represent the size of cloud droplet particles. Larger cloud droplets are more likely to form stronger icing when they touch the aircraft's surface. From Figure 6b, it can be seen that the spatial distribution of the large-value regions of effective particle radius is similar to that of the cloud liquid water path. The region where icing occurs is filled with large cloud droplet particles with an effective particle radius of larger than 14 μm, which is a favorable condition for icing. For the physical characteristics of clouds, the cloud-top temperature in the icing region (Figure 6c) is about −15 °C, from which it can be inferred that the temperature within clouds is around −10 °C. This temperature range not only indicates cold cloud characteristics but is also not too low, making it conducive to the existence of a large amount of supercooled water in low and medium clouds. Analyzing the optical thickness (Figure 6d), we found that the optical thickness of the icing area is greater than 70, and this area is covered by dense cold clouds, which is also consistent with the stratiform clouds described in the accident investigation report. The above-mentioned analysis has likewise verified the applicability of satellite remote sensing data in the identification of aircraft icing regions, and the application of satellite data will make up for the deficiency of icing observations.

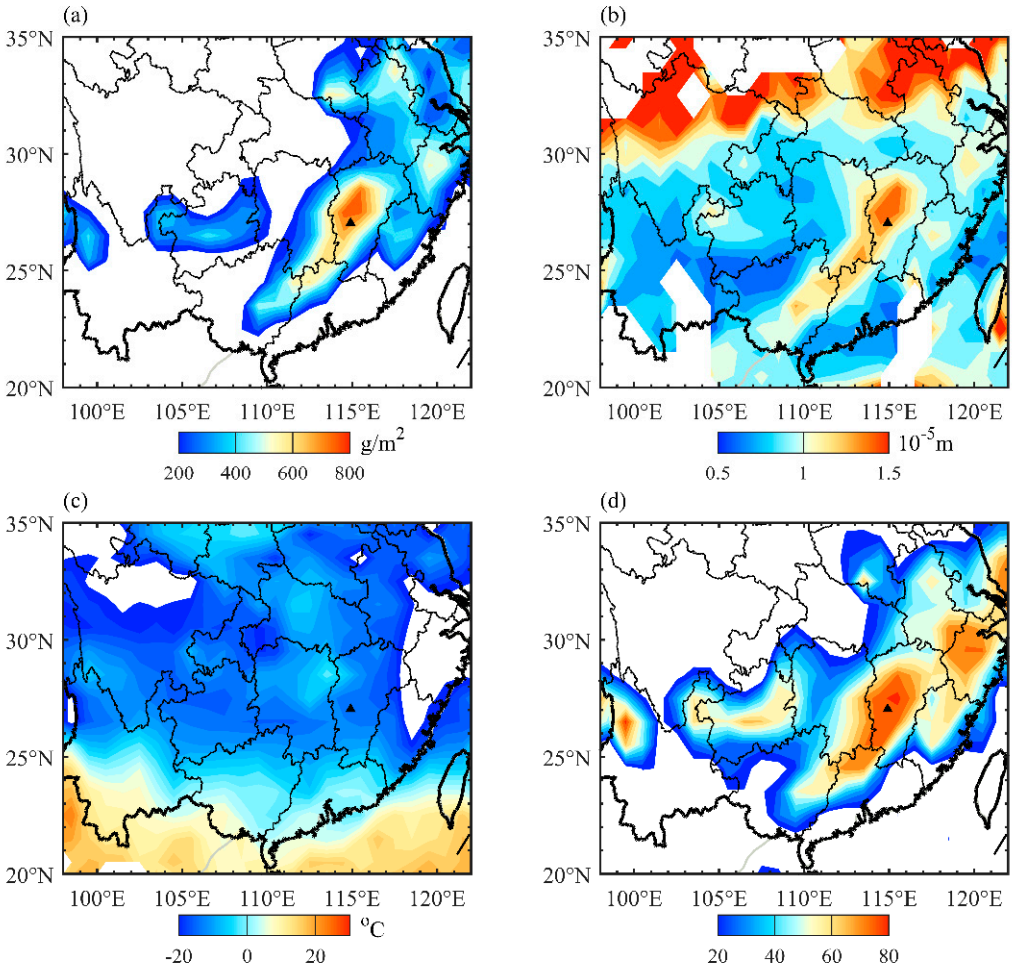

Figure 6. Spatial distributions of the (**a**) cloud liquid water path, (**b**) effective particle radius, (**c**) cloud top temperature, and (**d**) optical thickness from the Moderate-resolution Imaging Spectroradiometer observations on 1 March.

In addition to the stratiform cloud system produced by frontal uplifts, a large amount of latent heat released by adiabatic cooling of low-level water vapor can also alter the atmospheric stability, thus affecting the liquid water content in clouds. Figure 7 is a Skew-T Log-P diagram at 08:00 BJT on 1 March, which is based on the sounding data from Nanchang station (the closest to the accident location and in the same icing condition). From 925 hPa to 500 hPa, the ambient temperature profile is on the right side of the state curve, which indicates that the atmosphere is stable on the backside of the front under the influence of the frontal weather. At the same time, below 550 hPa, the dew point temperature difference is small, suggesting that the atmosphere is close to saturation. Such a stable atmospheric environment with temperature inversion at low levels weakens the convective exchange between the upper and lower layers, which is conducive to the accumulation of water vapor in clouds and temperature decrease, contributing to the formation of the large-value areas of the cloud water vapor path in Figure 6a.

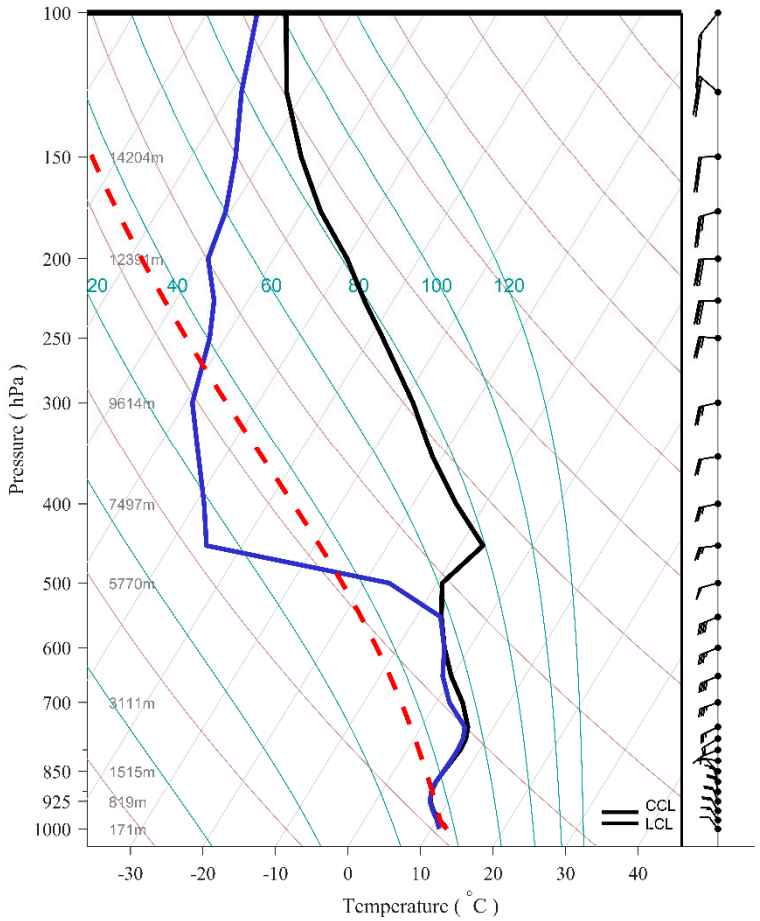

Figure 7. Skew-T Log-P diagram over Nanchang station at 08:00 BJT on 1 March. The thick black line indicates the ambient temperature profile, the thick blue line shows the dew point temperature profile, the red dotted line is the state curve, the gray lines are the isotherms, the brown lines are the dry adiabatic lines, and the green lines are the moist adiabatic lines.

The above analyses demonstrate that the upward motion along the front is the key to the icing meteorological conditions in a frontal process, both in terms of upward water vapor transport and the strengthening of the atmospheric stability behind the front. The vertical flow field (Figure 8a) at the incident location shows that there is strong vertical motion between 26° N and 28° N. Combined with the profile of pseudo-equivalent potential temperature (Figure 8b), it can be seen that the surface frontal line is located near 26° N. Therefore, in Figure 8a, the area near 27.5° N exhibits an apparent descending motion of cold air behind the front, and between 26° N and 27.5° N, there are tilted updrafts along the front from lower levels to 600–500 hPa above the incident location. In altitudes of 600–500 hPa, the pseudo-equivalent potential temperature is high, forming an obvious moist tongue, which shows the source of water vapor in the icing area. There are strong vertical water vapor fluxes along the front (Figure 8c). Specifically, in altitudes of 600–500 hPa, where the icing occurs, there are positive water vapor fluxes, suggesting that the water vapor is continuously transported from lower levels to upper levels along the inclined front. At 550 hPa, the water vapor flux convergence can be observed. It can be summarized that the upward motion along the cold front lifted the lower-level water vapor, leading to rapid moistening of the middle-level atmosphere above the incident location from 11:00 BJT to 15:00 BJT (Figure 4c). The warm-moist air enters the low-temperature zone to form a large amount of supercooled water droplets (Figure 6), which is conducive to the icing formation.

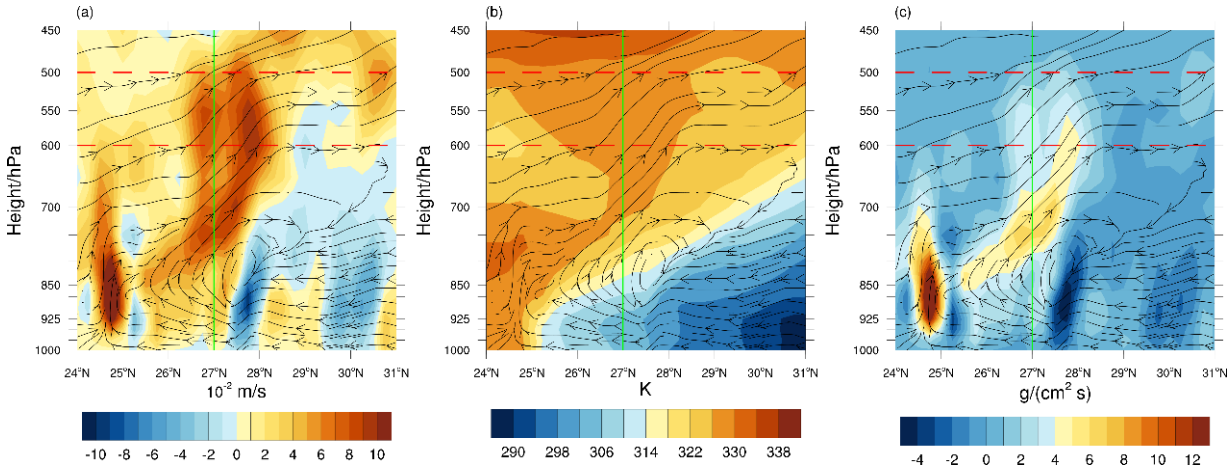

Figure 8. Height–latitude profiles of the meridional circulation (black streamline) superimposed on the (**a**) vertical velocity, (**b**) pseudo-equivalent potential temperature, and (**c**) water vapor flux across Ji'an City at 15:00 BJT on 1 March. The green lines show the latitude of the accident location, and the red dotted lines show the heights of 600 hPa and 500 hPa.

4. Numerical Simulations of Meteorological Conditions for the Aircraft Icing

The mesoscale numerical model is capable of accurately simulating frontal processes [52]. The WRF model is chosen to simulate the meteorological environment of this icing event, which can capture the formation process of supercooling water more accurately and depict the vertical distribution characteristics of supercooling water in the vicinity of the front more meticulously. At the same time, comparing the simulation results with the previous observational results can verify the capability of the WRF model to detect risky regions of aircraft icing. Using numerical models to provide icing forecasts and warnings for artificial weather modification operations is of great significance in the future. Figure 9a shows the simulated Ic index at 550 hPa at the moment of the incident. Compared with Figure 3c, we find that the model can well simulate the large-value regions of the Ic index in eastern China, particularly reproducing the large-value regions of the Ic index in the icing accident area (Simultaneously, the regional average Ic index obtained from the model is only 2% lower than the reanalysis observational data for Jiangxi Province). This result indicates that the WRF model effectively captures the icing weather conditions, laying a foundation for a detailed description of the formation process of icing environment. Additionally, the model reproduces the temperature, humidity and vertical wind fields over the incident location. As shown in Figure 9b, the southward movement of cold air and the high relative humidity areas extending upward along the front to 500 hPa are clearly visible. The ascending motion along the front can be found in Figure 9c.

Through the microphysical parameterization scheme, the model can describe the formation, growth, and disappearance of cloud droplets, as well as processes like condensation and evaporation in clouds. Therefore, the model can describe the formation processes of supercooled water, the most important meteorological condition for icing, under the influence of a cold front. As presented in Figure 10a, analyzing the Ic index, we found that the simulations obtained the same icing area as the observations (Figure 4a) at 600–550 hPa at the time of the incident. Moreover, on the north of the incident location, there is a continuous large-value area of the Ic index, which corresponds to the north–south oriented high-humid cold cloud zone detected by the satellite (Figure 6). Corresponding to the Ic index, the model identifies a high-value area of liquid water content within the icing area, as presented in Figure 10b. Compared with the satellite observations (Figure 6), the simulations more clearly depict the vertical structure of the large-value areas of the water vapor content, reflecting the vertical water vapor transport process by the front. Figure 10c displays that part of the water vapor transported to upper levels is transformed into solid ice crystals in the cool environment at high altitude, which is manifested as the large value

areas of ice water content. Solid ice crystals are less likely to adhere to the aircraft surface, thus making them less conducive to aircraft icing. However, Figure 10b,c suggests that compared with the large-value areas of liquid water content, those of ice water content are located farther north, situated in colder regions north of the icing accident area, thus having a lesser impact on the incident area. This suggests that the formation of the icing atmospheric environment is highly sensitive to temperature. Excessively low temperatures are also not conducive to the occurrence of aircraft icing, which demands that numerical models simulate the atmospheric temperature with great accuracy.

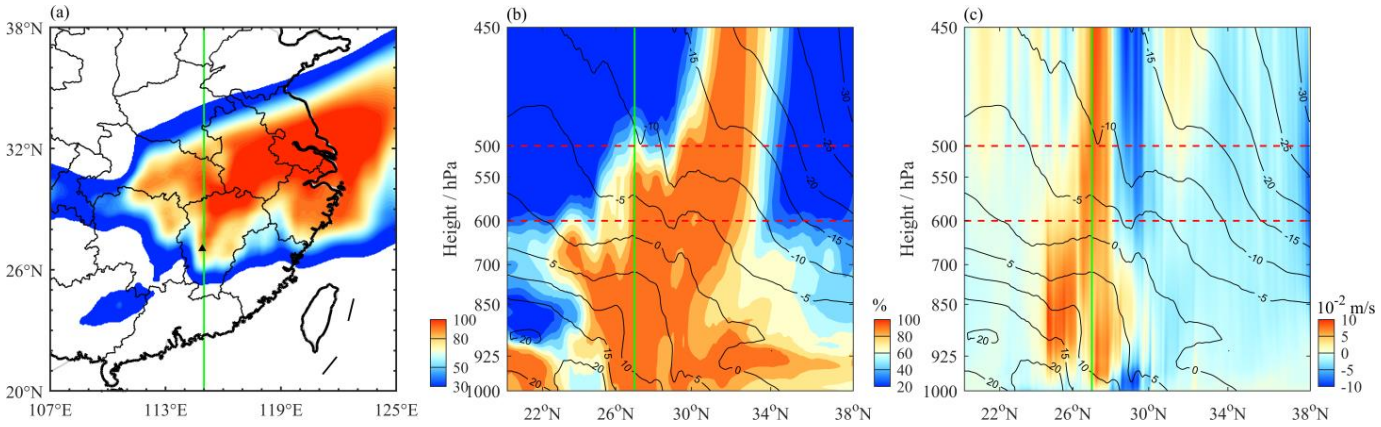

Figure 9. (**a**) Spatial distribution of the simulated Ic index at 500 hPa at 15:00 BJT on 1 March, and the meridional vertical sections (along the green line in (**a**)) of the corresponding (**b**) temperature (black solid lines), relative humidity, and (**c**) vertical velocity over the accident location. The green solid lines in (**b**,**c**) represent the latitude of the accident location, and the red dotted lines in (**b**,**c**) show the heights of 600 hPa and 500 hPa.

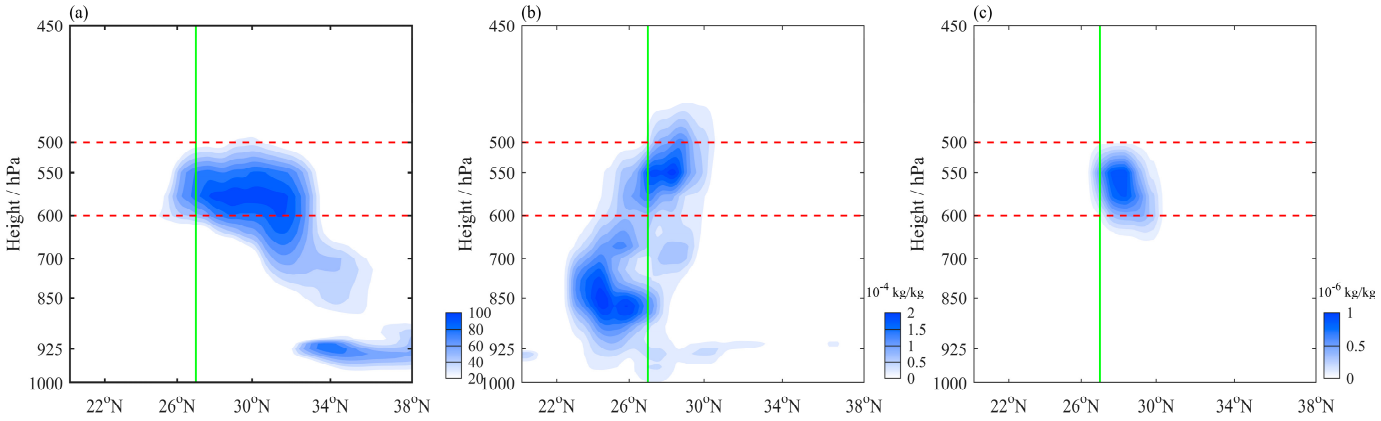

Figure 10. Meridional vertical section of the simulated (**a**) Ic index, (**b**) liquid water content, and (**c**) ice water content over the accident location at 15:00 BJT on 1 March.

The vertical profiles of the potential temperature and pseudo-equivalent potential temperature are used to portray the low-, middle-, and upper-level characteristics of the cold front, in order to further discuss the relationship between the vertical distribution of liquid water content and the frontal structure. From Figure 11a, it can be seen that from the surface to 850 hPa, the ground front characterized by dense equipotential temperature contours is located near 26° N. The incident location is located above the cold air behind the front. The large-value center of liquid water content is formed at 850 hPa. However, since the temperature at 850 hPa is above 0 °C without the formation of supercooled water, the Ic index is 0 (Figure 10a). The pseudo-equivalent potential temperature contours in Figure 11b show that the frontal slope is large, and thus water vapor rises rapidly along

the front. The low-level water vapor is transported to 600 hPa or above along the 325 K pseudo-equivalent potential temperature contour. At this height, the temperature ranges from −5 °C to −10 °C, and a large amount of supercooled water is generated, forming icing meteorological conditions.

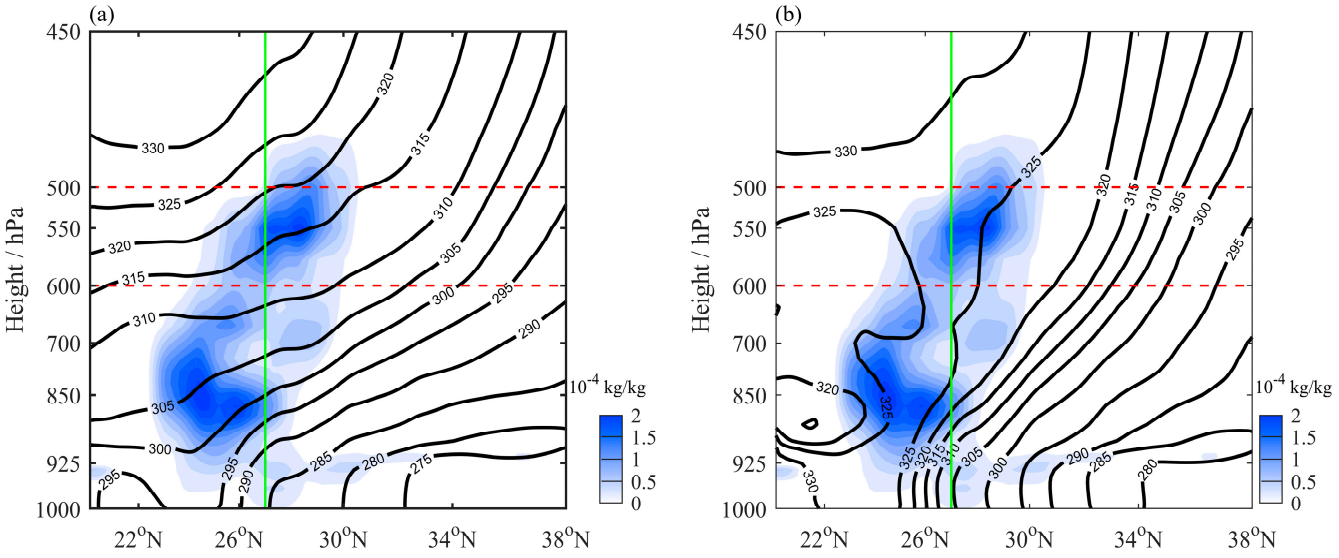

Figure 11. Same as Figure 10b, but with superimposed (**a**) potential temperature and (**b**) pseudo-equivalent potential temperature.

The vertical structure of each physical quantity output by the model can describe the relationship between the cold frontal process and the formation of icing meteorological conditions in upper levels. It is worth noting that the aircraft icing does not necessarily result in an immediate crash. The accident investigation report also mentioned that the aircraft was in icing conditions for an extended period, eventually resulting in severe icing that affected engine thrust and caused the crash. Different from some other weather systems such as severe convection, the icing-inducing atmospheric condition caused by the front is not short-lived but is continuous and widespread as the front moves. Figure 12 displays the altitude-time cross-sections of the simulated Ic index, vertical water vapor flux, liquid water content, and ice water content in Ji'an City from 07:00 BJT to 19:00 BJT on 1 March. The results indicate that with the passage of the cold front, the large-value areas of the Ic index appear near 550 hPa since 13:00 BJT on 1 March (Figure 12a). Meanwhile, the vertical water vapor transport strengthens as well (Figure 12b), which is reflected by the simultaneous increase of liquid water content (Figure 12c) and ice water content (Figure 12d). At this time, Ji'an City is influenced by the passage of the cold front, and the icing-inducing atmospheric environment forms over this region. Until 15:00 BJT, the above factors peak and last for nearly 2 h. During this period, the aircraft continued to fly in the environment, inevitably leading to serious aircraft icing.

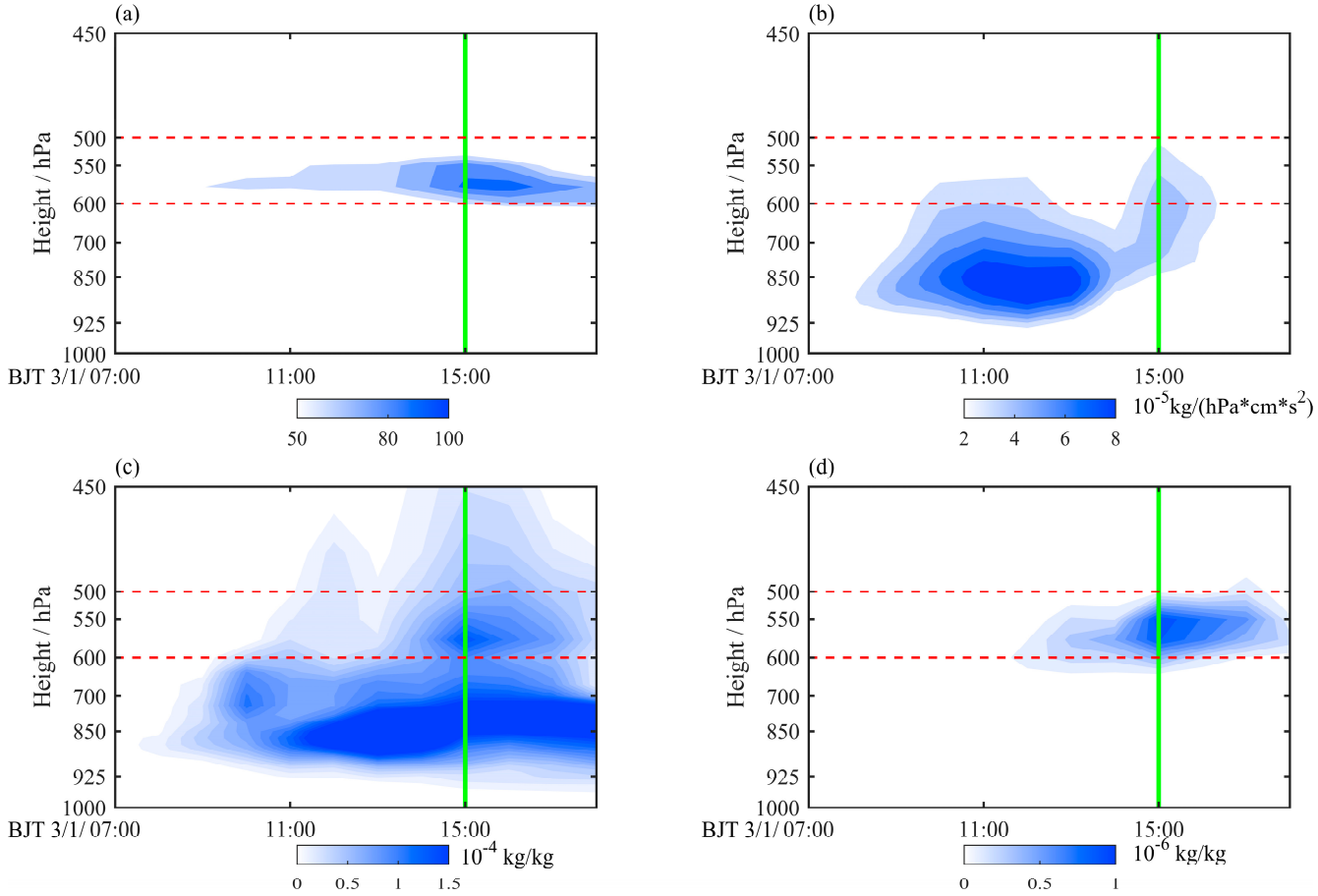

Figure 12. Altitude–time cross-sections of the simulated (**a**) Ic index, (**b**) vertical water vapor flux, (**c**) liquid water content, and (**d**) ice water content in Ji'an City from 07:00 BJT to 19:00 BJT on 1 March. The green solid lines represent the time of the accident, and the red dotted lines show the altitudes of 600 hPa and 500 hPa.

5. Conclusions

On 1 March 2021, an aircraft crash caused by icing occurred in Ji'an City, Jiangxi Province, China. This accident underscores the significant impact of meteorological factors related to aircraft icing on the flight safety of general aviation. Given the severity of the accident, the official investigation report extracted communication between the pilot and air traffic controller, as well as flight log data, to provide precise information regarding the time, location, altitude, and intensity of icing. This accident is a typical case for investigating the meteorological conditions for aircraft icing. Drawing on the investigation report of the accident, multi-source meteorological observations, and a numerical model, this research analyzes the meteorological conditions surrounding the aircraft icing incident. (Figure 13).

The main conclusions are as follows:

(1) Before the icing accident, a cold vortex combined with an upper-level trough led to the frontogenesis over the area from Qinghai to Shaanxi. Subsequently, the cold front moved from northwest to southeast, passing through the north of Jiangxi Province on the day of the incident. Consequently, the icing area was primarily influenced by the cold frontal process at the time of the accident. At the same time, since the incident location was situated east of the southwest vortex, the warm advection from the ocean made the low-level water vapor sufficient.

(2) The investigation report shows that the aircraft icing happened at an altitude range of 4800–5100 m. At 550 hPa, the strong correlation between the large-value center of the Ic index and the movement of the cold front suggests that the icing environment is closely associated with the cold front. Analyzing the two key meteorological factors, temperature,

and humidity, we found that the warming ahead of the front increased the temperature slightly at the altitude of the accident, but as the ambient temperature was too low, the temperature condition could still lead to icing. Moreover, warm-moist updrafts along the front increased the relative humidity at 600–500 hPa, and thus, the water vapor condition for icing was satisfied, leading to the formation of an icing-prone atmospheric environment.

(3) Analyzing the temperature variations, cloud liquid water path, effective particle radius, cloud top temperature, optical thickness, temperature and humidity profiles, and vertical flow field, it is found that aircraft icing occurred behind the ground front. The frontal circulation transported water vapor from lower levels to upper levels, which caused the development of cold stratiform clouds. A significant number of large cloud droplets were generated within the clouds, and the frontal inversion contributed to atmospheric stability. Thus, cloud droplets accumulated in the low-temperature region above 600 hPa and formed supercooled water droplets. As a result, the aircraft experienced severe icing under these meteorological conditions.

(4) The WRF model well reproduces the atmospheric environment of this icing event. Based on the simulated liquid water content, the formation process of supercooled water, a critical condition for icing, is analyzed under the influence of the frontal processes.

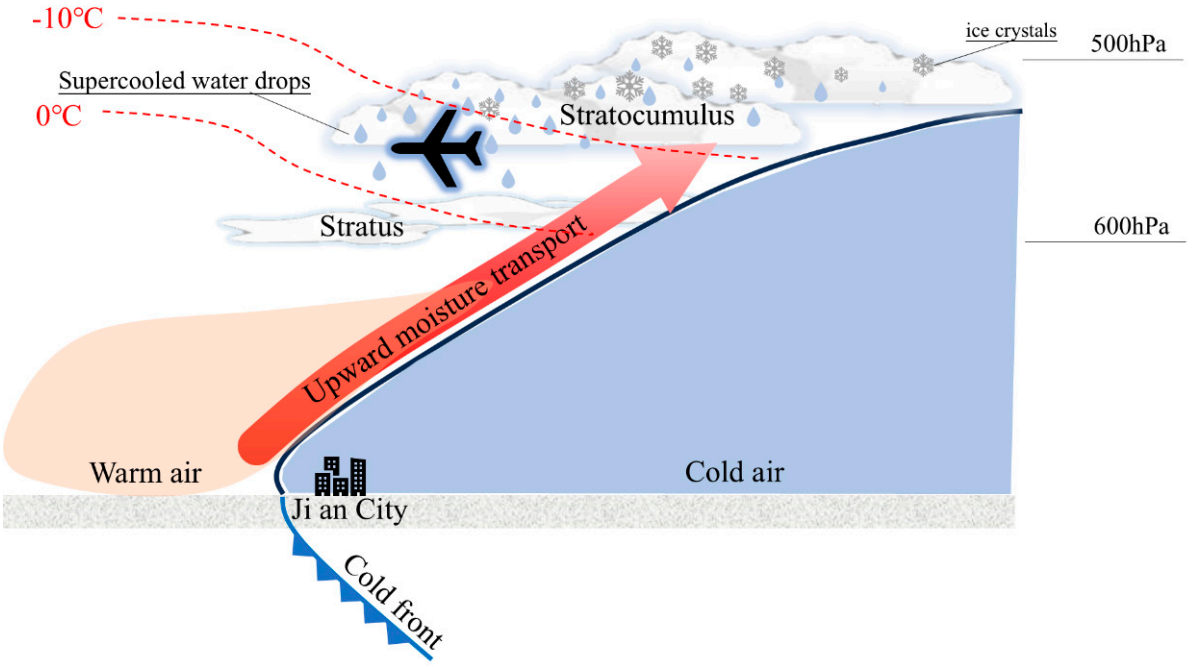

Figure 13. Conceptual model of the weather conditions for aircraft icing formation under the influence of a cold front.

We developed a conceptual model of the meteorological conditions for aircraft icing influenced by a frontal system, based on a typical case study (Figure 13), and evaluated the performance of the WRF model in simulating icing-related meteorological conditions under frontal influence. This research aims to provide a theoretical foundation and practical reference for future meteorological support regarding aircraft icing in general aviation.

This study benefited from the open usage of multi-source meteorological data. The free-of-charge and free-accessible data and tools (such as the ERA5 and MODIS datasets, the WRF model, and the official accident investigation report from CAAC) made it feasible to conduct this research, highlighting the significance of data sharing. However, due to the lack of direct airborne observations of cloud physical characteristics, this study relied more on reanalysis data and satellite observations, which did not provide sufficiently detailed descriptions of hydrometeors in the actual atmospheric environment. Therefore, future research will employ airborne detection equipment such as cloud droplet probes and cloud

particle image probes to conduct precise observations of icing-inducing meteorological elements, allowing for the correction of icing forecast models and better management of icing risks.

Author Contributions: Conceptualization, H.L. and C.M.; methodology, Z.L. and H.L.; data curation, R.F. and Z.L.; writing—original draft preparation, H.L. and S.P.; project administration, T.W. and L.D.; funding acquisition, Y.L. All authors have read and agreed to the published version of the manuscript.

Funding: This work was jointly supported by the Fundamental Research Funds for the Central Universities (No. J2023-034); the Open Foundation of China Meteorological Administration Key Laboratory for Aviation Meteorology (No. HKQXM-2024018); the National Key R&D Program of China (No. 2021YFB2601701).

Data Availability Statement: The raw data supporting the conclusions of this article will be made available by the authors on request.

Acknowledgments: We thank the five anonymous reviewers for their comments and suggestions. We would also like to thank ECMWF for offering the ERA5 dataset, NASA LP DAAC for making MODIS data freely available, and ORNL DAAC for providing the MODIS Land Product Subsets web service. The Mesoscale and Microscale Meteorology Laboratory (MMM) of NCAR for supporting the WRF system to the user community, and for maintaining the WRF code on GitHub.

Conflicts of Interest: The authors declare no conflict of interest.

References

1. Cao, Y.; Tan, W.; Wu, Z. Aircraft icing: An ongoing threat to aviation safety. *Aerosp. Sci. Technol.* **2018**, *75*, 353–385. [CrossRef]
2. Yamazaki, M.; Jemcov, A.; Sakaue, H. A Review on the Current Status of Icing Physics and Mitigation in Aviation. *Aerospace* **2021**, *8*, 188. [CrossRef]
3. Zhou, C.; Li, Y.; Zheng, W.; Wu, P.; Dong, Z. Safety Analysis for Icing Aircraft during Landing Phase Based on Reachability Analysis. *Math. Probl. Eng.* **2018**, *2018*, 3728241. [CrossRef]
4. Sundaresan, A.; Arunvinthan, S.; Pasha, A.A.; Pillai, S.N. Effect of Ice accretion on the aerodynamic characteristics of wind turbine blades. *Wind Struct.* **2021**, *32*, 205–217.
5. Lynch, F.T.; Khodadoust, A. Effects of ice accretions on aircraft aerodynamics. *Prog. Aerosp. Sci.* **2001**, *37*, 669–767. [CrossRef]
6. Cao, Y.; Wu, Z.; Su, Y.; Xu, Z. Aircraft flight characteristics in icing conditions. *Prog. Aerosp. Sci.* **2015**, *74*, 62–80. [CrossRef]
7. Bromfield, M.A.; Horri, N.; Halvorsen, K.; Lande, K. Loss of control in flight accident case study: Icing-related tailplane stall. *Aeronaut. J.* **2023**, *127*, 1554–1573. [CrossRef]
8. Boyd, D.; Guinn, T. Deficiencies in Safe Practices by Pilots Operating General Aviation Aircraft in Weather Conducive for Icing. *J. Aviat. Technol. Eng.* **2024**, *13*, 13–22. [CrossRef]
9. Kind, R.J.; Potapczuk, M.G.; Feo, A.; Golia, C.; Shah, A.D. Experimental and computational simulation of in-flight icing phenomena. *Prog. Aerosp. Sci.* **1998**, *34*, 257–345. [CrossRef]
10. Czernkovich, N. Understanding in-flight icing. In Proceedings of the Transport Canada Aviation Safety Seminar, Budapest, Hungary, 17 November 2004; pp. 1–21.
11. Bragg, M.B.; Basar, T.; Perkins, W.R.; Selig, M.S.; Voulgaris, P.G.; Melody, J.W.; Sarter, N.B. Smart Icing Systems for Aircraft Icing Safety. In Proceedings of the 40th AIAA Aerospace Sciences Meeting and Exhibit, Reno, NV, USA, 14–17 January 2002; pp. 1–16.
12. Hauf, T.; Schröder, F. Aircraft icing research flights in embedded convection. *Meteorol. Atmos. Phys.* **2005**, *91*, 247–265. [CrossRef]
13. Merino, A.; García-Ortega, E.; Fernández-González, S.; Díaz-Fernández, J.; Quitián-Hernández, L.; Martín, M.L.; López, L.; Marcos, J.L.; Valero, F.; Sánchez, J.L. Aircraft Icing: In-Cloud Measurements and Sensitivity to Physical Parameterizations. *Geophys. Res. Lett.* **2019**, *46*, 11559–11567. [CrossRef]
14. Sand, W.R.; Cooper, W.A.; Politovich, M.K.; Veal, D.L. Icing Conditions Encountered by a Research Aircraft. *J. Clim. Appl. Meteorol.* **1984**, *23*, 1427–1440. [CrossRef]
15. Nickovic, S.; Cvetkovic, B.; Petković, S.; Amiridis, V.; Pejanović, G.; Solomos, S.; Marinou, E.; Nikolic, J. Cloud icing by mineral dust and impacts to aviation safety. *Sci. Rep.* **2021**, *11*, 6411. [CrossRef]
16. Bernstein, B.C.; Le Bot, C. An Inferred Climatology of Icing Conditions Aloft, Including Supercooled Large Drops. Part II: Europe, Asia, and the Globe. *J. Appl. Meteorol. Climatol.* **2009**, *48*, 1503–1526. [CrossRef]
17. Li, S.; Qin, J.; He, M. Fast Evaluation of Aircraft Icing Severity Using Machine Learning Based on XGBoost. *Aerospace* **2020**, *7*, 36. [CrossRef]
18. Schultz, P.; Politovich, M.K. Toward the Improvement of Aircraft-Icing Forecasts for the Continental United States. *Weather Forecast.* **1992**, *7*, 491–500. [CrossRef]
19. Thompson, G.; Bruintjes, R.T.; Brown, B.G.; Hage, F. Intercomparison of In-Flight Icing Algorithms. Part I: WISP94 Real-Time Icing Prediction and Evaluation Program. *Weather Forecast.* **1997**, *12*, 878–889. [CrossRef]

20. Bernstein, B.C.; McDonough, F.; Politovich, M.K.; Brown, B.G.; Ratvasky, T.P.; Miller, D.R.; Wolff, C.A.; Cunning, G. Current Icing Potential: Algorithm Description and Comparison with Aircraft Observations. *J. Appl. Meteorol.* **2005**, *44*, 969–986. [CrossRef]
21. Morcrette, C.; Brown, K.; Bowyer, R.; Gill, P.; Suri, D. Development and Evaluation of In-Flight Icing Index Forecast for Aviation. *Weather Forecast.* **2019**, *34*, 731–750. [CrossRef]
22. Fernández-González, S.; Sánchez, J.L.; Gascón, E.; López, L.; García-Ortega, E.; Merino, A. Weather Features Associated with Aircraft Icing Conditions: A Case Study. *Sci. World J.* **2014**, *2014*, 279063. [CrossRef]
23. Reinking, R.F.; Snider, J.B.; Coen, J.L. Influences of Storm-Embedded Orographic Gravity Waves on Cloud Liquid Water and Precipitation. *J. Appl. Meteorol.* **2000**, *39*, 733–759. [CrossRef]
24. Bernstein, B.C.; Omeron, T.A.; McDonough, F.; Politovich, M.K. The Relationship between Aircraft Icing and Synoptic-Scale Weather Conditions. *Weather Forecast.* **1997**, *12*, 742–762. [CrossRef]
25. Politovich, M.K.; Bernstein, T.A.O. Aircraft Icing Conditions in Northeast Colorado. *J. Appl. Meteorol.* **2002**, *41*, 118–132. [CrossRef]
26. Politovich, M.K. Aircraft Icing Caused by Large Supercooled Droplets. *J. Appl. Meteorol.* **1989**, *28*, 856–868. [CrossRef]
27. Smith, W.L., Jr.; Minnis, P.; Young, D.F. An icing product derived from operational satellite data. In Proceedings of the Ninth Conference on Aviation, Range and Aerospace Meteorology, Orlando, FL, USA, 13 September 2000; pp. 256–259.
28. Tafferner, A.; Hauf, T.; Leifeld, C.; Hafner, T.; Leykauf, H.; Voigt, U. ADWICE: Advanced Diagnosis and Warning System for Aircraft Icing Environments. *Weather Forecast.* **2003**, *18*, 184–203. [CrossRef]
29. Nicholls, S. A model of drizzle growth In warm, turbulent, stratiform clouds. *Q. J. R. Meteorol. Soc.* **2007**, *113*, 1141–1170. [CrossRef]
30. Wang, X.; Zhang, J.; Wang, S. Climatic Features of Aircraft Icing of China. *Meteorol. Sci.* **2002**, *22*, 343–350. (In Chinese)
31. Wang, J.; Xie, B.; Cai, J. The Distribution of Aircraft Icing Accretion in China—Preliminary Study. *Atmosphere* **2020**, *11*, 876. [CrossRef]
32. Li, Z. Analysis of meteorological conditions of aircraft icing. *J. Sichuan Meteor.* **1999**, *19*, 55–57. (In Chinese)
33. Pang, Z.; Zhang, Y. Weather Conditions of Aircraft Icing in the Middle Part of Gansu Province. *Arid Meteor.* **2008**, *26*, 53–56. (In Chinese)
34. Sun, J.; Cai, M.; Wang, F.; Shi, Y. A case study of aircraft icing conditions in Anqing Area. *Meteor. Mon.* **2019**, *45*, 1341–1351. (In Chinese)
35. Chi, Z. Statistical Analysis and Numerical Prediction Experiment of Weather Conditions for Aircraft Icing. *Meteor. Sci. Technol.* **2007**, *33*, 714–718+766. (In Chinese)
36. Wang, Z.; Zhou, X.; Wu, J.; Li, B.; Lin, Y.; Yan, W.; Zhang, Y. Weather Conditions and Cloud Microphysical Characteristics of an Aircraft Severe Icing Process. *J. Appl. Meteor. Sci.* **2022**, *33*, 555–567. (In Chinese)
37. Sun, J.; Tan, C.; Zhou, Y.; Liu, Z.; Huang, J.; Wang, Z. Meteorological Conditions of Two Cases of Aircraft Icing in Spring in Xinjiang. *Meteor. Environ. Sci.* **2021**, *44*, 24–32. (In Chinese)
38. Nygaard, B.E.K.; Kristjánsson, J.E.; Makkonen, L. Prediction of In-cloud icing conditions at ground level using the WRF model. *J. Appl. Meteorol. Climatol.* **2011**, *50*, 2445–2459. [CrossRef]
39. Regmi, R.P.; Kitada, T.; Dudhia, J.; Maharjan, S. Large-Scale Gravity Current over the Middle Hills of the Nepal Himalaya: Implications for Aircraft Accidents. *J. Appl. Meteorol. Climatol.* **2017**, *56*, 371–390. [CrossRef]
40. Davis, N.; Hahmann, A.N.; Clausen, N.-E.; Žagar, M. Forecast of Icing Events at a Wind Farm in Sweden. *J. Appl. Meteorol. Climatol.* **2014**, *53*, 262–281. [CrossRef]
41. Guo, Q.; Sang, W.; Niu, J.; Yi, Z.; Xia, Z.; Miao, S. Evaluation of Different Cloud Microphysics Schemes on the Meteorological Condition Prediction of Aircraft Icing. *Trans. Nanjing Univ. Aeronaut. Astronaut.* **2023**, *40*, 124–136.
42. Bian, S.; An, H.; Su, X.; Huang, Y. Diagnostic Analysis and Intensity Prediction Modeling of Aircraft Icing Process. *Meteor. Disaster Reduct. Res.* **2023**, *46*, 304–311. (In Chinese)
43. Ratvasky, T.P.; Barnhart, B.P.; Lee, S. Current Methods Modeling and Simulating Icing Effects on Aircraft Performance, Stability, Control. *J. Aircraft.* **2010**, *47*, 201–211. [CrossRef]
44. Hersbach, H.; Bell, B.; Berrisford, P.; Hirahara, S.; Horányi, A.; Muñoz-Sabater, J.; Nicolas, J.; Peubey, C.; Radu, R.; Schepers, D.; et al. The ERA5 global reanalysis. *Q. J. R. Meteorol. Soc.* **2020**, *146*, 1999–2049. [CrossRef]
45. Dyroff, C.; Zahn, A.; Christner, E.; Forbes, R.; Tompkins, A.M.; van Velthoven, P.F.J. Comparison of ECMWF analysis and forecast humidity data with CARIBIC upper troposphere and lower stratosphere observations. *Q. J. R. Meteorol. Soc.* **2014**, *141*, 833–844. [CrossRef]
46. Belo-Pereira, M. Comparison of in-flight aircraft icing algorithms based on ECMWF forecasts. *Meteorol. Appl.* **2015**, *22*, 705–715. [CrossRef]
47. Skamarock, W.C.; Klemp, J.B. A time-split nonhydrostatic atmospheric model for weather research and forecasting applications. *J. Comput. Phys.* **2008**, *227*, 3465–3485. [CrossRef]
48. Bolgiani, P.; González, S.F.; Martin, M.L. Analysis and numerical simulation of an aircraft icing episode near Adolfo SuárezMadrid-Barajas International Airport. *Atmos. Res.* **2017**, *200*, 60–69. [CrossRef]
49. Liu, T.; Sun, J.; Zhou, Y.; Peng, C.; Yan, F. Simulation Study on Stratiform Cloud Structure of Trough Cold Front and Characeristics of Supercooled Water Distribution. *Meteor. Mon.* **2015**, *41*, 1232–1244. (In Chinese)
50. Wu, J.J.; Yang, C.J.; Xun, R.R.; Wang, L.; Yu, W.F.; Chen, Q. Analysis of Aircraft Icing Characteristics in Sichuan Basin Based on Cloudsat Data. *Aeronaut. Comput. Tech.* **2023**, *53*, 24–28. (In Chinese)

51. Zhou, X.X.; Li, Y.Y.; Zhang, C. Study on the Forecasting Method and Application Scenario of Aircraft Icing. *Meteor. Mon.* **2023**, *49*, 415–426. (In Chinese)
52. Mierzwiak, M.; Kroszczynski, K.; Araszkiewicz, A. WRF Parameterizations of Short-Term Solar Radiation Forecasts for Cold Fronts in Central and Eastern Europe. *Energies* **2023**, *16*, 5136. [CrossRef]